A&A 405, 1063–1074 (2003)
DOI: 10.1051/0004-6361:20030643

Astronomy & Astrophysics

The massive binary CPD – 41° 7742 I. High-resolution optical spectroscopy⋆

H. Sana[1,⋆⋆], H. Hensberge[2], G. Rauw[1,⋆⋆⋆], and E. Gosset[1,⋆⋆⋆]

[1] Institut d'Astrophysique et de Géophysique, Université de Liège, Allée du 6 Août 17, Bât. B5c, 4000 Liège, Belgium
e-mail: sana@astro.ulg.ac.be
[2] Royal Observatory of Belgium, Ringlaan 3, 1180 Brussels, Belgium
e-mail: Herman.Hensberge@oma.be

Received 28 February 2003 / Accepted 23 April 2003

Abstract. We present the results of a spectroscopic campaign on the early-type binary CPD – 41° 7742. For the first time, we unambiguously detect the secondary's spectral signature and derive an accurate orbital solution for both components of the system. We confirm that the orbit displays a slight but definite eccentricity ($e = 0.027 \pm 0.006$) despite the short period ($P = 2.44070 \pm 0.00043$ days). Previous radial velocity measurements available in the literature constitute together with our new observations a data set that spans more than 30 years. The combined primary orbital solution inferred is in excellent agreement with our solution and gives a period $P = 2.44062 \pm 0.00005$ days. Based on spectroscopic criteria, we derive a spectral and luminosity classification of O9 III + B1 III. However, the luminosities and radii inferred from the membership of NGC 6231 rather indicate lower luminosity classes. We show that the equivalent widths of well isolated primary lines display variations that suggest that CPD – 41° 7742 is an eclipsing binary. This makes CPD – 41° 7742 the second known SB2 eclipsing early-type binary of the NGC 6231 cluster. We approximately constrain the inclination of the system $i_{\rm min} \approx 60°$. This may indicate that the system does not offer enough room for two stars with radii typical of giant stars and lends further support to a less evolved luminosity classification for at least one of the objects.

Key words. stars: individual: CPD – 41° 7742 – stars: binaries: close – stars: binaries: spectroscopic – stars: early-type – stars: fundamental parameters

1. Introduction

Early-type stars of spectral type O and Wolf-Rayet are among the hottest and most luminous objects of our Galaxy and play a crucial role in numerous galactic issues such as the galactic evolution. Massive stars are essential sources of ultraviolet and ionizing radiation. Their influence on their surroundings is also mechanical and results from their huge stellar winds associating large terminal velocities with enormous mass-loss rates. They can even trigger giant star formation events (Maeder & Meynet 1995; Deharveng et al. 2003). However, despite their importance, our understanding of these objects is still far from satisfactory and more accurate observational data are needed to constrain the theoretical models. Indeed parameters as essential as the mass and the mass-loss rates are still poorly constrained, not to mention the rotation (Maeder & Meynet 2000). The studies of binaries in open stellar clusters is of special relevance for our understanding of star formation processes, dynamical interaction in clusters and stellar evolution in general (Gimenez 1996). In this context, we undertook a multiwavelength observing campaign on several stars of the NGC 6231 cluster in the core of the Sco OB 1 association. The project combines optical and XMM X-ray data and aims at providing a homogeneous set of observational constraints on the physical parameters of a sample of O-type stars. This first paper about CPD – 41° 7742 is devoted to the spectroscopic analysis of the system. One aim is to obtain contemporaneous accurate ephemerides that are needed to correctly interpret the X-ray data. Another is to derive reliable physical and orbital parameters of the system.

CPD – 41° 7742 ($V = 8.32$, Baume et al. 1999) is an early-type spectroscopic binary that belongs to the young open cluster NGC 6231. Commonly used alternative names are CD–41°11042, Braes 945 (Braes 1967), Seggewiss 224 (alternatively S 224, Seggewiss 1968), V1034 Sco (Kukarkin et al. 1971), Sung 505 (alternatively SBL 505, Sung et al. 1998) and Baume 11 (alternatively BVF 11, Baume et al. 1999). This object was first suspected to be a binary by Struve (1944) on the

Send offprint requests to: H. Sana, e-mail: sana@astro.ulg.ac.be
⋆ Based on observations collected at the European Southern Observatory (La Silla, Chile).
⋆⋆ Research Fellow FNRS (Belgium).
⋆⋆⋆ Research Associate FNRS (Belgium).

Table 1. Journal of the spectroscopic observations of CPD – 41° 7742. Column 1 reports the heliocentric Julian Date at mid-exposure. The next three columns give the phases as calculated from the He I λ4471 orbital solution as well as the radial velocities (*RV*s) of the primary (Col. 3) and secondary (Col. 4) as measured from the Doppler shifts of the He I λ4471 line. A similar structure is adopted for the last three columns. $\phi_{\overline{\text{He I}}}$ reports the phases computed from the average He I solution (see Sect. 3.3). $\overline{RV_1 - \gamma_{\lambda,1}}$ and $\overline{RV_2 - \gamma_{\lambda,2}}$ present the values obtained by averaging the *RV*s of He I lines measured on the FEROS spectra. Prior to averaging, the *RV*s have been corrected for the systemic velocities of the individual lines (see Table 3). The phase $\phi = 0.0$ corresponds to the time of periastron passage as given in the corresponding orbital solutions of Table 4.

Hel. Jul. Date (−2 450 000)	$\phi_{\text{He I }\lambda4471}$	RV_1 (km s^{-1})	RV_2 (km s^{-1})	$\phi_{\overline{\text{He I}}}$	$\overline{RV_1 - \gamma_{\lambda,1}}$ (km s^{-1})	$\overline{RV_2 - \gamma_{\lambda,2}}$ (km s^{-1})
995.723	0.549	119.4	−271.8			
996.654	0.931	−82.6	−82.6			
997.669	0.347	−79.7	26.7			
998.657	0.751	84.4	−226.8			
999.664	0.164	−185.9	231.2			
1000.642	0.565	126.4	−278.2			
1299.843	0.154	−188.4	283.6	0.129	−163.9	289.1
1300.841	0.563	131.5	−275.4	0.538	155.0	−273.9
1301.847	0.975	−137.3	173.4	0.950	−108.9	198.5
1302.847	0.385	5.4	−113.6	0.360	23.8	−40.5
1304.841	0.202	−163.5	218.1	0.177	−137.1	255.8
1327.863	0.635	142.8	−308.4	0.609	167.6	−296.9
1668.928	0.377	3.4	−101.5	0.350	22.3	−37.3
1669.791	0.730	99.6	−257.2	0.703	125.1	−230.7
1669.923	0.784	64.3	−187.3	0.758	79.8	−154.4
1670.787	0.138	−192.3	281.0	0.112	−169.3	293.3
1670.901	0.185	−173.3	221.7	0.158	−152.1	265.4
1671.800	0.553	123.5	−274.9	0.527	147.6	−268.6
1671.926	0.605	142.0	−295.9	0.578	162.4	−295.1
1672.782	0.956	−122.7	164.5	0.929	−92.7	185.8
1672.925	0.014	−167.1	206.9	0.988	−138.9	244.1
2037.792	0.509	102.1	−254.7	0.480	128.3	−232.9
2037.887	0.547	123.1	−278.6	0.519	146.2	−272.6
2039.783	0.324	−65.5	n.	0.296	−56.3	54.4
2039.907	0.375	−23.2	−23.2	0.347	2.6	13.1
2040.788	0.736	100.3	−243.5	0.708	121.3	−220.3
2040.908	0.785	71.7	−146.5	0.757	87.9	−138.7
2337.860	0.453	69.9	−194.6	0.424	91.6	−167.8
2338.794	0.836	21.6	−114.2	0.806	49.2	−72.2
2381.723	0.425	46.7	−116.8	0.395	64.1	−103.4
2382.741	0.842	15.6	−104.2	0.812	40.9	−64.9
2383.738	0.250	−131.4	180.2	0.221	−105.6	204.9

basis of only two spectra. A few decades later, from a set of sixteen observations, Hill et al. (1974, HCB74 hereafter) determined a period of $P = 2.446 \pm 0.005$ days and a low eccentricity of $e = 0.07 \pm 0.04$. Only the primary component was detected and the semi-amplitude of the radial velocity curve was found to be $K_1 = 162.5 \pm 8.2\,\mathrm{km\,s^{-1}}$. These authors also reported a photometric variability of $\Delta V = 0.45$ mag. Levato & Malaroda (1980) assigned a spectral type of O9 IV and, with four more observations, Levato & Morrell (1983, hereafter LM83) determined $P = 2.430155 \pm 0.00001$ days, $e = 0.08 \pm 0.03$, $K_1 = 160 \pm 5\,\mathrm{km\,s^{-1}}$, $v \sin i = 130\,\mathrm{km\,s^{-1}}$. In 1990, Perry et al. (1990, PHYB90 hereafter) published three more radial velocity (*RV*) points obtained in the late 1960s, but no new orbital solution. Finally, García & Mermilliod (2001, GM01 hereafter) recently claimed to have detected the secondary spectral signature on three out of their eight new medium resolution spectra. Combining these new data with the previous measurements reported in the literature, they proposed a first SB2 solution for the system. They adopted a longer period $P = 2.453087 \pm 0.000012$ days and, contrasting with previous papers, derived a quite large eccentricity ($e = 0.205$) for such a short period. However, we will show in Sect. 4 that this option

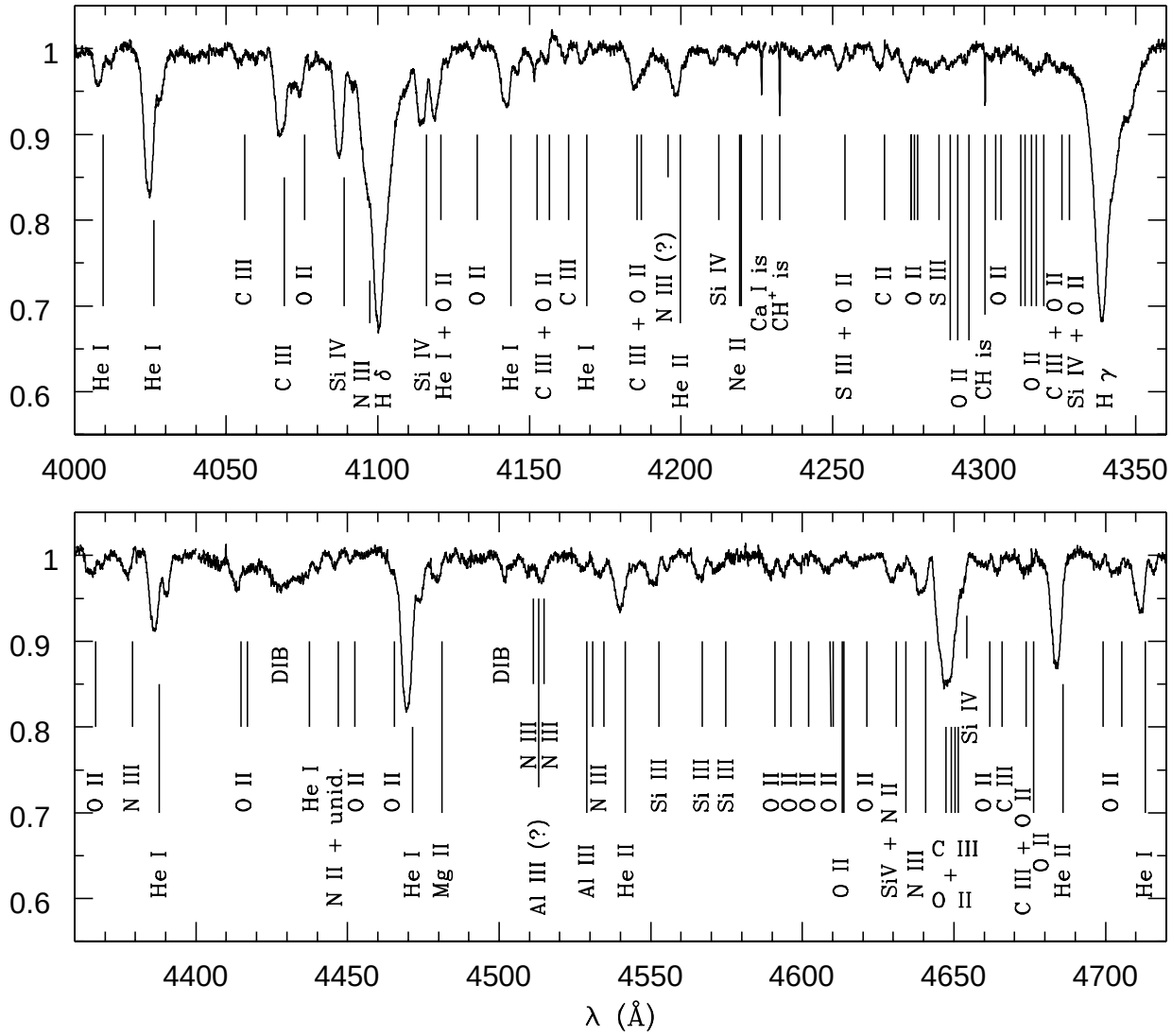

Fig. 1. Blue spectrum of CPD – 41° 7742 as obtained on HJD = 2 452 383.738 ($\phi_{\overline{\text{He I}}} = 0.221$). The identification of the main lines has been indicated. He I lines display a clear SB2 signature, with the blue-shifted primary and the red-shifted secondary components. The identification ticks refer to the rest wavelengths.

is erroneous and we will provide an alternative global orbital solution for the system.

This paper is organized as follows. In the next section, we first describe both our data set and the reduction processes that we applied. Section 3 is devoted to the determination of the orbital motion of the system. In Sect. 4, we combine our data with previous observations reported in the literature. We pay particular attention to the discrepancies between GM01 results and ours. In Sect. 5, we discuss the physical parameters and the evolutionary status of the binary components. The last section summarizes our main conclusions.

2. Observations and data reduction

2.1. Observations

The present work is based on 32 high-resolution spectra of CPD – 41° 7742 obtained at the European Southern Observatory (ESO, La Silla, Chile). These were acquired during 25 nights distributed over 7 runs between July 1998 and April 2002. The journal of the observations is presented in Table 1.

In July 1998, six spectra in the range 4460–4480 Å (He I λ4471) were obtained at the ESO 1.4 m Coudé Auxiliary Telescope (CAT), with the Coudé Echelle Spectrograph (CES) equipped with the Very Long Camera (VLC). The detector used was ESO CCD#38, a Loral 2688 × 512 pixel CCD with a pixel size of 15 μm × 15 μm. The slit width was chosen to achieve a nominal resolving power of 70 000–80 000. The effective resolving power as derived from the *FWHM* of the lines of the ThAr calibration exposures is 65 000–75 000. Typical exposure times were 40 min and the average S/N ratio is about 100.

Between April 1999 and April 2002, we collected 26 spectra covering the whole optical range (3800–9200 Å) using the FEROS echelle spectrograph mounted at the ESO 1.5 m telescope at La Silla. The detector was a 2k×4k EEV CCD with

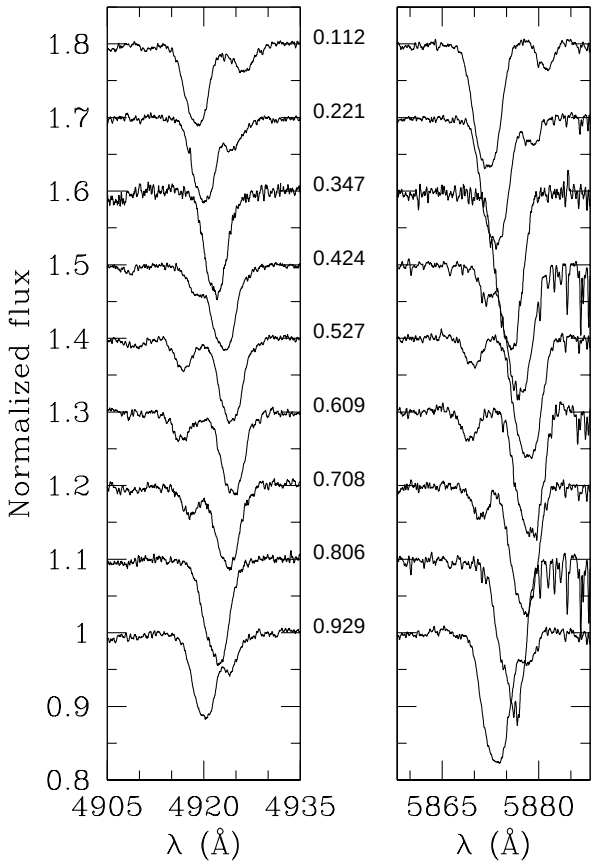

Fig. 2. He I λ4922 (left) and He I λ5875 (right) lines at various phases. The numbers in between the two panels give the phases $\phi_{\overline{\text{He I}}}$ at mid-exposure. The spectra were shifted along the vertical axis for the sake of clarity. The secondary spectral signature is clearly identified on most spectra but the blended ones.

a pixel size of 15 μm × 15 μm. The spectral resolving power of FEROS is 48 000. Typical exposure times were 30 min, resulting in typical S/N of about 150 and 180 at 4200 Å and 6000 Å respectively. During the two runs of May 2000 and 2001, we obtained two spectra per night, separated by a few hours (typically 3 to 4 h), in order to solve the period aliasing that a preliminary analysis of the data had revealed.

2.2. Data reduction

CES data were reduced in a standard way using the MIDAS package supported by ESO. The spectra were then rectified by means of an instrumental response curve built from the observations, obtained under similar conditions, of a metal-poor "reference" star (HD 203608: F6V). Finally, the spectra were normalized by fitting a low order polynomial (a straight line or a parabola) to the continuum.

FEROS data were reduced using the FEROS context working under MIDAS environment. We found that the standard pipe-line reduction failed to provide satisfactory results (Hensberge 2002). Based on the expertise of one of the authors (HH), we locally implemented an improved reduction pipe-line that allows a more accurate wavelength calibration (with rms residuals down to 3.0×10^{-3} Å), a better correction for the diffused background light and hence an improved determination of the blaze functions that, in the basic reduction case, displayed "oscillations" due to the flat-field calibration lamps. These oscillations, not present in the stellar spectra, were therefore a major source of uncertainty in the determination of the continuum. Finally, artefacts due to the merging of the echelle orders of the FEROS data are known to appear in a number of order reconnections. This problem, added to the complexity of the global shape of the spectrograph response curve, renders the normalization step a non-trivial process. For these reasons, we performed the normalization both on the merged spectra and on the individual orders separately, and we carefully compared both resulting normalized spectra to avoid any anomaly due to the automatic FEROS merging. In some cases, we also used a reference star with few metallic lines (either HD 152248 or 9 Sgr), observed and reduced under similar conditions, to build an instrumental response curve. This allowed us to perform an additional check of the normalization process.

Table 2. Period search carried out with the Lafler & Kinman (L&K) and Fourier (HMM, see text) techniques and based on the *RV*s associated with the He I λ4471 (upper part of the table) and O III λ5592 (lower part) lines. The last column gives the value either of the normalized L&K statistic or of the Fourier semi-amplitude at the given optimum period.

Data set	Method	Period (d)	Θ_1 / $A_{\max}$
He I λ4471: RV_1	L&K	2.44084	0.036
RV_2		2.44067	0.060
RV_1–RV_2		2.44067	0.055
RV_1	HMM	2.44065	164
RV_2		2.44076	291
RV_1–RV_2		2.44075	460
O III λ5592: RV_1	L&K	2.44052	0.084
RV_1	HMM	2.44064	162

3. CPD – 41° 7742 spectrum and orbital solution

3.1. The spectrum of CPD – 41° 7742

The spectrum of CPD – 41° 7742 (see Fig. 1) is clearly dominated by the Balmer lines and by the He I and He II absorption lines. Numerous metallic lines (C, N, O, Si and Mg ions) can also be identified. The Balmer lines and all the He I lines in the observed wavelength range present a clear SB2 signature with the primary lines being several times stronger than the associated secondary lines (see e.g. Fig. 2). No emission line is detected in the CPD – 41° 7742 spectrum.

We first measured the line positions, and thus the Doppler shifts, and we computed the radial velocities (*RV*s) associated with the main lines of the spectra. We then used them to deduce a new SB2 orbital solution for the system. For this purpose, we selected well isolated lines and measured the line positions by fitting Gaussians to the studied profiles. Depending on the separation of the double (SB2) lines, one or two Gaussians were simultaneously adjusted. Whenever possible, we attempted to separate blended lines using templates of both primary and secondary lines built on the basis of the large *RV*-separation spectra. The method has been described in Rauw et al. (2000).

Table 3. Orbital solutions deduced from different *RV* data sets. The usual notations for the orbital elements have been used. s_y/s_x is the ratio of the relative uncertainties associated to secondary and primary *RV*s respectively. ω is the primary longitude of periastron. A "n" indicates that the related element has no relevance as a better agreement with the data has been reached assuming a circular orbit. Quoted uncertainties are the 1-σ error bars.

Lines	P (d)	s_y/s_x	e	ω (°)	K_1 (km s^{-1})	K_2 (km s^{-1})	γ_1 (km s^{-1})	γ_2 (km s^{-1})	rms (km s^{-1})
He I λ4009	2.44066	1.7	n.	n.	157.7 ± 2.5	302.1 ± 4.7	−2.8 ± 2.6	−13.1 ± 4.3	10.1
He I λ4026	2.44065	2.1	0.022 ± 0.011	112 ± 34	165.2 ± 2.2	295.5 ± 4.0	−14.9 ± 2.1	−14.7 ± 3.0	8.4
He I λ4471	2.44068	2.3	0.046 ± 0.009	139 ± 14	168.5 ± 1.7	291.9 ± 2.9	−23.8 ± 1.6	−22.6 ± 2.1	8.4
He I λ4922	2.44075	2.1	0.042 ± 0.008	167 ± 8	169.8 ± 1.5	296.6 ± 2.6	−11.0 ± 1.3	−34.0 ± 1.7	6.9
He I λ5016	2.44067	2.2	0.026 ± 0.005	99 ± 16	169.4 ± 1.2	306.5 ± 2.2	−16.4 ± 1.1	−29.7 ± 1.6	5.2
He I λ5048	2.44070	2.3	0.027 ± 0.015	190 ± 21	169.9 ± 2.3	310.3 ± 4.1	−17.3 ± 2.2	−35.4 ± 3.1	9.8
He I λ5875	2.44069	2.4	0.026 ± 0.005	122 ± 12	168.4 ± 1.0	304.0 ± 1.7	−15.3 ± 0.9	−23.4 ± 1.2	4.2

Due to the presence of numerous metallic lines, some interesting lines are usually blended with neighbouring ones. In those cases where the line profiles are effectively affected by the surrounding lines, we carried out simultaneous multi-Gaussian fits. To compute the *RV*s associated with the measured Doppler shifts, we mostly adopted the effective wavelengths for O-stars from Conti et al. (1977) below 4800 Å and from Underhill (1994) above. For the metallic lines that are typically not present in O-star spectra, we used rest wavelengths from Moore (1959). A selection of He I *RV* measurements is presented in Table 1.

3.2. Period determination

As a next step, we searched for the period P of the orbital motion. For this purpose, we applied both the method of Lafler & Kinman (1965, L&K hereafter) and the Fourier analysis of Heck et al. (1985, HMM hereafter; see also Gosset et al. 2001 for comments). The period search algorithms were applied on the data sets associated with the He I λ4471 and O III λ5592 lines. The first set is the most extensive with 32 observations and offers thus the largest time base. However, the He I λ4471 lines are most of the time blended with the O II λ4465 and Mg II λ4481 lines. Primary and secondary lines are also heavily blended near conjunction phases. On the other hand, the O III λ5592 is a single line that is associated with the primary component. It is also well isolated in the spectrum of CPD – 41° 7742. Consequently, though it is a fainter line ($EW \approx 0.16$ Å), its position can be well determined at all phases. Period values, obtained with Lafler & Kinman and Fourier analyses, based on different *RV* sets are reproduced in Table 2. The He I λ4471 time base is $T = 1388$ d, leading to a natural width of the peak in the power spectrum of $\Delta\nu = 1/T = 0.00072\,\mathrm{d}^{-1}$ and a corresponding resolution on the quoted period value $\Delta P = 0.0043$ d. The full width at half maximum in the periodogram gives $\Delta P = 0.0039$ d, as expected from the theoretical value. Adopting a final uncertainty of one tenth of the peak width, we obtain $\sigma_P = 4\,10^{-4}$ d. Following a similar reasoning, the uncertainty on the O III λ5592 associated period is 5×10^{-4} d. Period values given in Table 2 do well agree within their uncertainties.

3.3. Orbital solutions

We used a modified version of the Wolfe et al. (1967) algorithm to compute new orbital solutions based on various lines. Beyond the general philosophy of the modifications implemented and described in Rauw et al. (2000), new considerations hold in the case of a binary with two components that have quite different luminosities. Indeed in such a situation where the primary and secondary lines could not be adjusted with a similar accuracy (e.g. due to a significant brightness difference), it is necessary to attribute a different relative weighting to the primary and secondary *RV*s. In our derived solutions, we adopted a period value and a relative primary to secondary weight ratio that yield the lowest residuals. Table 3 displays the deduced orbital parameters depending on the selected lines. These are in a quite acceptable agreement from one line to the other.

Finally, we computed the average *RV*s of all the quoted He I lines by shifting the individual *RV*s to a common centre, taking into account the systemic velocities deduced from the individual orbital solutions. This combined curve gives a better accuracy and the fit will be adopted as our final SB2 solution for the physical and orbital parameters, and for the ephemerides. The values of the corresponding variables are given in Table 4. Figure 3 illustrates this average He I line solution. In the following, we briefly compare our results with previously published solutions.

1. Period: The period values deduced from our different data sets are in excellent agreement. Their mean value is $P = 2.44069 \pm 0.00003$ d, with a standard deviation one order of magnitude below the period uncertainty deduced from the power spectrum peak width. This period is considered as equivalent to the adopted value $P = 2.44070$ d reported in Table 4. Our period is therefore situated between the two extreme values of LM83 (2.430155 d) and of GM01 (2.45087 d), but is closer to a previous determination by HCB74 (2.446 d). Periods around 2.430 and 2.450 days are incompatible with our data set.

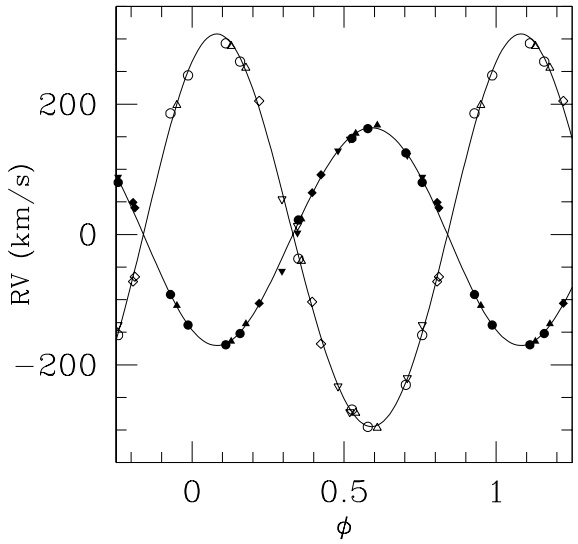

Fig. 3. Phase diagram giving the *RV* curves corresponding to the average He I line solution in the *zero systemic velocity* reference frame. Measured *RV* points associated with the primary (filled symbols) and secondary (open symbols) components are overplotted. Different symbols refer to different observation periods: upward triangles = CES 1998; squares = FEROS 1999; circles = FEROS 2000; downward triangles = FEROS 2001; diamonds = FEROS 2002.

2. Eccentricity: Values for the eccentricity (resp. the longitude of periastron passage ω) from the different data sets show some dispersion that might be related to the difficulty to accurately determine a low eccentricity along with corresponding time of periastron passage in such a system. However, if we except the case of the He I λ4009 line, a better agreement between the *RV* curves and the observations is obtained adopting a slightly eccentric orbit rather than a circular one. Primary individual *RV* solutions from O III λ5592 and He II λ4686 confirm a moderate eccentricity. Though HCB74 and LM83 already suggested a low eccentricity for the system, GM01 proposed a much larger eccentricity $e = 0.205$, clearly in disagreement with our independently derived orbital solution. We will discuss this discrepancy more into details in the next section.

3. Systemic velocities: Weighted average values for *apparent* systemic velocities are -15.3 ± 0.5 and $-26.3 \pm 0.7\,\mathrm{km\,s^{-1}}$ for the primary and secondary respectively. The quoted errors give the uncertainties on the mean values, while the actual scatter (standard deviation) of the present sample of systemic velocities is about 4.5 and 6.4 $\mathrm{km\,s^{-1}}$ for γ_1 and γ_2 respectively. Comparing these values with the mean error on the individual systemic velocities may suggest that either the latter are underestimated or that our measurements suffer from some source of systematic error. Mainly, such non-random errors may originate from non-Gaussian profiles of the studied lines or from slightly different effective rest wavelengths than those we used. For these reasons, we choose to refer the measured *RV*s to a *zero systemic velocity* reference frame prior to averaging. Finally, primary *apparent* systemic velocities are on average 10 $\mathrm{km\,s^{-1}}$ more positive than secondary ones. These mean values will be taken into account when comparing our average He I solution and *RV* points with other "uncorrected" data.

Table 4. Orbital and physical parameters of CPD – 41° 7742 as deduced from different data sets: our data on He I λ4471, on the average over selected He I lines (see Sect. 3) and a data set extended by primary *RV*s found in the literature (see Sect. 4).

	He I λ4471	He I lines	Lit.
P (d)	2.44068	2.44070	2.44062
s_y/s_x	2.3	2.1	n.
m_1/m_2	1.728 ± 0.024	1.803 ± 0.015	n.
e	0.046 ± 0.009	0.027 ± 0.006	0.030 ± 0.017
ω (°)	139 ± 14	149 ± 10	27 ± 31
T_0 (HJD −2 450 000)	2400.212 ±0.092	2400.284 ±0.067	2399.444 ±0.208
K_1 ($\mathrm{km\,s^{-1}}$)	168.5 ± 1.7	167.1 ± 0.9	161.2 ± 2.5
K_2 ($\mathrm{km\,s^{-1}}$)	291.9 ± 2.9	301.3 ± 1.8	n.
γ_1 ($\mathrm{km\,s^{-1}}$)	−23.8± 1.6	0.7 ± 0.9	−16.0 ± 1.8
γ_2 ($\mathrm{km\,s^{-1}}$)	−22.6 ± 2.1	−0.6 ± 1.3	n.
$a_1 \sin i$ ($R_\odot$)	8.13 ± 0.08	8.05 ± 0.05	7.77 ± 0.12
$a_2 \sin i$ ($R_\odot$)	14.05 ± 0.14	14.52 ± 0.09	n.
$m_1 \sin^3 i$ ($M_\odot$)	15.61 ± 0.37	16.69 ± 0.25	n.
$m_2 \sin^3 i$ ($M_\odot$)	9.03 ± 0.19	9.25 ± 0.12	n.
rms ($\mathrm{km\,s^{-1}}$)	8.4	4.8	13.1

4. An orbital solution combining (new and) published data

This section presents a combined study of the CPD – 41° 7742 *RV* measurements adding those reported in the literature. The journal of the published observations is presented in Table 5. We excluded however Struve's (1944) data from our survey because of their much poorer quality. As the reader may have noticed at this point, there are some major discrepancies between our orbital solution and the one of García & Mermilliod (GM01). Before attempting to combine all the data available, we first need to clarify this point.

4.1. GM01's data and their orbital solution

GM01 data result from CASLEO optical observations with the REOSC-SEL[1] echelle spectrograph. They observed the spectral range between 3750 and 4861 Å. The REOSC-SEL resolving power is about ∼14 000. The S/N ratio was between 50 and 80 for a typical exposure time of 30 min. Concerning CPD – 41° 7742, they reported to have carried out *RV* measurements, on average, on 15 lines for the primary component, whereas they worked with 10, 11 and 2 lines for the three secondary observations. This might correspond to Balmer and He I lines for the secondary, adding He II lines for the

[1] Spectrograph Echelle Liège – jointly built by REOSC and Liège observatory and on long-term loan from the latter.

Table 5. Journal of the observations of CPD – 41° 7742 reported in the literature. Column 1 gives the heliocentric Julian Date. Column 2 gives the phases as calculated from the average He I orbital solution (see Sect. 3). Columns 3 and 4 report the radial velocities (*RV*s), respectively associated with the primary (Col. 3) and secondary (Col. 4) components. Column 5 indicates the origin of the data. cGM01 stands for corrected GM01 data (see text).

Hel. Jul. Date (−2 400 000)	$\phi_{\overline{\text{He I}}}$	RV_1 (km s^{-1})	RV_2 (km s^{-1})	Source
39959.792	0.900	47.0		PHYB90
40018.810	0.081	−92.0		
40019.833	0.500	0.0		
40807.734	0.318	−114.0		HCB74
40808.632	0.685	166.4		
40809.479	0.032	−55.5		
40809.568	0.069	−98.8		
40809.690	0.119	−132.2		
40810.532	0.464	−40.6		
40812.486	0.265	−166.2		
40812.642	0.328	−142.9		
40813.481	0.672	145.8		
40813.587	0.716	145.0		
40813.703	0.763	151.0		
40814.510	0.094	−129.5		
40815.500	0.499	−9.4		
40815.595	0.538	21.3		
40817.479	0.310	−150.4		
40817.677	0.391	−71.3		
43647.711	0.909	13.3		LM83
43648.775	0.345	−125.0		
43649.765	0.750	144.0		
43650.789	0.170	−164.0		
49912.743	0.808	36.5		cGM01
49914.521	0.537	127.5		
49915.538	0.954	−127.8	145.5	
49967.537	0.258	−94.8		
50593.680	0.801	6.6		
50594.726	0.229	−129.2	193.0	
50596.827	0.090	−162.8	195.9	
50597.811	0.493	115.8		

primary. Excluding the point where the secondary is only detected in 2 lines does not solve the observed discrepancies.

First of all, we tried to reproduce the GM01 solution, which is presented in their Fig. 1 (labelled 505). However, the number of *RV* points presented in their orbital solution seems to be much smaller than what they claimed to have used. Our Fig. 4 (left panel) presents what should be an equivalent figure. It is clear that several *RV* points have been discarded when GM01 plotted their figure, i.e. one secondary *RV* point (out of three) and other HCB74 points around GM01 phase 0.7 are missing. PHYB90 *RV* points are not plotted on their figure either. The latter points clearly disagree with GM01 orbital solution (see Fig. 4, left panel). Finally, it is clear from Fig. 4 (right panel) that our *RV* points are incompatible with GM01 period and orbital solution.

According to Mermilliod (2003), some of the Julian Dates reported in GM01 are wrong by one day and should be corrected by subtracting one day to the published dates. Their

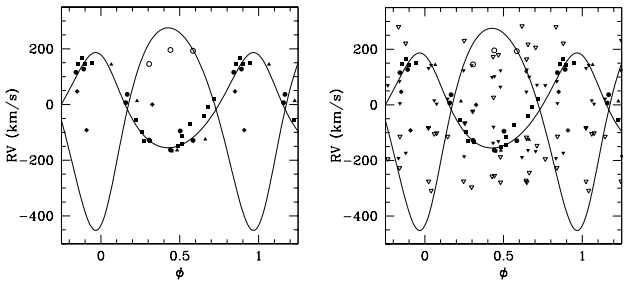

Fig. 4. Phase diagrams based on the ephemerides of GM01 (P = 2.453087 d). Different observational points are also plotted along with the orbital solution suggested by GM01. *Left*: Published primary (filled symbols) and secondary (open symbols) *RV* points: diamonds = PHYB90, squares = HCB74, triangles = LM83, circles = GM01. *Right*: idem but our He I λ4471 *RV* points have been added (downward triangles). The latter ones do obviously not match the orbital solution proposed by GM01.

proposed solution is therefore spurious, as is the high eccentricity found. Once the one-day shift is applied to the last four observations reported by GM01, the corrected GM01 data (cGM01) reach a good agreement with previous and new observations. The Julian Dates quoted in Table 5 have therefore been corrected accordingly to prevent further erroneous use of these data.

4.2. Combined period determination

As a next step, we tested our period and solution against published *RV* values. This is presented in Fig. 5. A small shift is visible between our solution and the position of PHYB90, HCB74 and LM83 measurements. This shift might result either from a small uncertainty on the period or from the ill-constrained time of periastron passage that we adopted as phase zero. Note that a similar shift could also arise from an apsidal motion of a slightly eccentric orbit. However all these data points seem in acceptable agreement with a shifted version of our *RV* curve. The cGM01 data are almost contemporaneous with ours and the primary *RV*s present a better agreement with our orbital solution. However we observe a large amplitude difference between cGM01 secondary points and our solution. This probably comes from the poorer resolution and S/N ratio of their spectra which prevent accurate *RV* measurements for the fainter component.

In addition, we applied the L&K method and the HMM Fourier analysis on different data sets, combining our *RV*s with published measurements, in order to find a common value for the period. For this purpose, we only used primary *RV* points. As the primary lines are much more intense than the secondary ones, the bias resulting from the blending of primary and secondary lines on lower resolution spectra should not too strongly affect primary *RV* measurements. Results are summarized in Table 6. We observe that the values for the period deduced either from the combined data set (P = 2.44062 d) or from our different sets (cf. Tables 3 and 4) are in very good agreement.

The next paragraph presents a primary orbital solution as computed by combining our new data with all previous

Table 6. Period searches carried out with the L&K and HMM methods and based on published primary *RV* points combined with our new measurements. The first column indicates the data set used. The second gives the number of *RV* points in the set. Columns 3 and 4 provide the period found and the relevant normalized statistic of the L&K method. The next two columns report similar values obtained from the HMM Fourier analysis. $A_{\rm max}$ is the semi-amplitude of the Fourier term. The last two columns present the time base of the set and the uncertainty on the L&K period as supposed to correspond to one tenth of the natural width of the peak. The uncertainties on the HMM values are of the same order of magnitude. cGM01 stands for corrected GM01 data as quoted in Table 5.

		L&K		HMM			
Data set	n	P (d)	Θ_1	P (d)	$A_{\rm max}$	Time base (d)	σ_P (d)
cGM01	8	2.440634	0.404	2.440586	152	686	8.7×10^{-4}
PHYB90+HCB74+LM83	23	2.440611	0.077	2.440646	156	3691	1.6×10^{-4}
PHYB90+HCB74+LM83+cGM01	31	2.440619	0.049	2.440615	155	10639	4.2×10^{-5}
cGM01+this work	40	2.440709	0.033	2.440683	161	2471	2.4×10^{-4}
PHYB90+HCB74+LM83+this work	55	2.440620	0.023	2.440627	161	12424	4.8×10^{-5}
All the available data	63	2.440619	0.019	2.440626	160	12424	4.8×10^{-5}

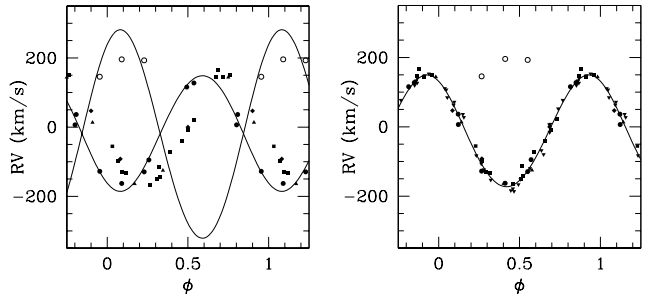

Fig. 5. Phase diagrams based on our ephemerides and orbital solutions as given in Table 4. *Left*: Published primary (filled symbols) and secondary (open symbols) *RV* points overplotted on our average He I line *RV* curves. Phases have been calculated from the average He I line ephemerides (P = 2.44070 d). *Right*: combined primary orbital solution. Corresponding orbital elements are presented in Table 4 in the column labelled "Lit." (P = 2.44062 d). In both panels the symbols have the same meaning: diamonds = PHYB90, squares = HCB74, triangles = LM83, circles = corrected GM01, downward triangles = this work.

RV measurements that we were able to find in the literature, except those from Struve (1944).

4.3. A global orbital solution for the primary

A *RV* curve that combines published data with those of the present work is presented in Fig. 5 (right panel) and the corresponding orbital solution is given in Table 4. A very good agreement is found with our derived solution. We emphasize that the literature *RV* points combined with ours provide a time base T of 12 424 days. This corresponds to a theoretical peak width in the power spectrum of $\Delta\nu = 1/T = 8.0\times10^{-5}\,{\rm d}^{-1}$, giving $\Delta P = 4.8\times10^{-4}$ d. The observed width of the peak is in good agreement with that value. Finally, the combined data set gives a period of $P = 2.44062 \pm 0.00005$ d.

In conclusion, we showed that the reported GM01 data were problematic and incompatible with previous and new observations of CPD – 41° 7742. This results from the use of erroneous Julian Dates. The period and eccentricity that GM01 derived using their set of data is therefore not correct. Shifting some of the reported HJD by one day as suggested by Mermilliod (2003) solves the observed discrepancies and allows us to include the corrected GM01 data in the combined solution. Finally, the other *RV* measurements found in the literature are in excellent agreement with our results and therefore reinforce the confidence that we have in our newly derived SB2 solution.

5. Physical parameters ofCPD – 41° 7742

5.1. Spectral types and luminosity classes

5.1.1. Primary component

The spectral signature of the primary component is easily discernible in the spectrum of CPD – 41° 7742. We adopted the classification criteria from Conti (1973) as adapted to late O-stars by Mathys (1988); they are based on the equivalent width (EW) ratio of the He I λ4471 and He II λ4542 lines. He I λ4471 EWs were only measured on spectra obtained at large *RV* separation phases. We obtain a mean $\log W'(\frac{W_{\lambda4471}}{W_{\lambda4542}}) = 0.42\pm0.04$ which corresponds to a spectral type O9, with spectral type O9.5 within $1\,\sigma$.

To determine the luminosity class, we adopted the criterion from Conti & Alschuler (1971) based on the EW ratio of the Si IV λ4089 and He I λ4144 lines. We obtain $\log W''(\frac{W_{\lambda4089}}{W_{\lambda4144}}) = 0.24\pm0.04$, which leads to a giant luminosity class. We are also aware of Mathys criterion based on $\log W''' = \log(W_{\lambda4388}) + \log(W_{\lambda4686})$. However, as it is based on the product of absolute EWs and not on their relative ratio, we first need to estimate the optical brightness of both components of the system (see Sect. 5.2).

5.1.2. Secondary component

The main spectral signatures of the secondary star in CPD – 41° 7742 are the Balmer and He I lines for which we were able to measure the positions and EWs with a good confidence. We also note the absence of He II lines, as well as of the O III λ5592 line, at the positions predicted by the orbital solution (see e.g. Fig. 6). The absence of He II lines definitively excludes an O spectral type and, at our detection threshold, most probably indicates a spectral subtype later than B0.7 (Walborn & Fitzpatrick 1990, WF90 hereafter).

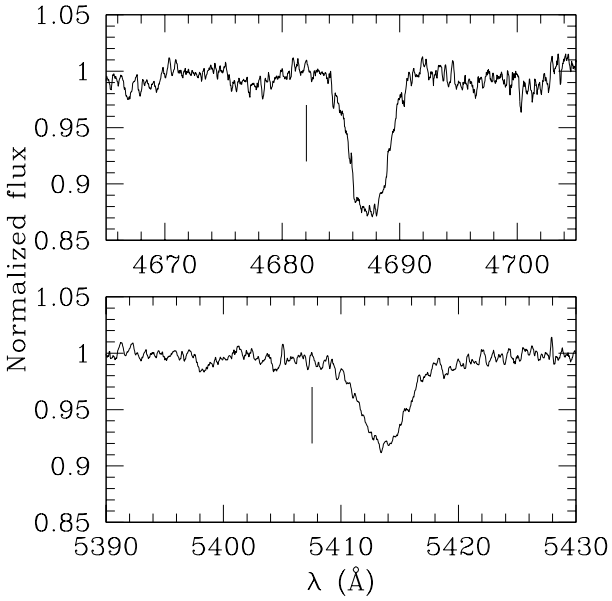

Fig. 6. He II λ4686 (upper panel) and He II λ5412 (lower panel) lines in the spectra obtained respectively at $\phi_{\overline{\text{He I}}} = 0.48$ and $\phi_{\overline{\text{He I}}} = 0.71$. The vertical marks indicate the expected position of the secondary line according to our orbital solution.

Table 7. Identified metallic lines associated to the secondary component of CPD – 41° 7742. First column gives the identified ion. The second and third columns respectively report the mean equivalent width (*EW*) of the line and the rest wavelength adopted for *RV* computations. The uncertainties quoted in Col. 2 are the 1 σ dispersions of our measurements.

Line	*EW* (Å)	Rest wavelength (Å)
Si IV λ4089	0.067 ± 0.012	4088.863
Si III λ4253[a]	0.022 ± 0.009	4253.593
C II λ4267	0.030 ± 0.012	4267.02
O II λ4367	0.029 ± 0.011	4366.896
N III λ4379	0.020 ± 0.011	4379.09
Mg II λ4481	0.028 ± 0.014	4481.228
Si III λ4552	0.051 ± 0.021	4552.654

[a] Most probably blended with the O II $\lambda\lambda$4253.74-53.98 lines.

To refine our subtype classification, we carefully searched for the presence of secondary metallic lines in our FEROS spectra. This led us to consider low intensity lines, with *EW*s down to ~0.02 Å, and we therefore excluded spectra with too low S/N. Numerous metallic lines associated with the primary (and thus statistically more intense than the relevant secondary lines) render this task even more delicate. The results that we present in Table 7 only concern the lines that could unambiguously be associated with the secondary orbital motion (see e.g. Figs. 7 and 8) and do not pretend to be exhaustive.

WF90 suggest to use the Si III λ4552/He I λ4388 (resp. Si III λ4552/Si IV λ4089) ratio for the luminosity (resp. spectral type) classification of B0-3 stars. From our measurements, we obtained 0.44 ± 0.20 (resp. 0.76 ± 0.34). Comparing the CPD – 41° 7742 secondary spectrum to the OB atlas of WF90, the first criterion definitively excludes a supergiant luminosity class. This is reinforced by the low intensity of the secondary O II spectrum. The same criterion, though with a lower confidence, also seems to indicate a giant luminosity class rather than classes V or IV. Finally the ratio Si III λ4552/Si IV λ4089 tends to favor spectral type B1 compared to B2. We are then left with a O9 III + B1 III classification for the CPD – 41° 7742 system.

5.2. Optical brightness ratio

We roughly estimated the optical brightness ratio based on the dilution of the primary lines in the spectrum of CPD – 41° 7742. For this purpose, we compared mean *EW*s of primary lines with typical (averaged) *EW*s of O9 III stars (Conti & Alschuler 1971; Conti 1973). Based on the He I $\lambda\lambda$4026, 4388, 4471 and He II λ4542 lines, we respectively obtained a brightness ratio of $l_1 = \frac{L_1}{L_{\rm tot}} = 0.97, 0.98, 0.87$ and 0.86. Mean value is then $l_1 = 0.92 \pm 0.06$. Note that He II λ4686 is even more intense in CPD – 41° 7742 global spectrum than on average O9 III spectra and may thus rather indicate a class V for the primary star. Comparing secondary intrinsic *EW*s with typical *EW*s for B star (Didelon 1982) gives $l_2 \sim 0.1$, at the B1-B3 peak, for the He I lines. Together with C II, Mg II and Balmer lines, the same test implies $l_2 \leq 0.14$ and confirms a B1-3 V-III class for the secondary.

Adopting $l_1 = 0.92 \pm 0.06$, $W^{\rm obs}_{\lambda 4388} = 351 \pm 25$ mÅ and $W^{\rm obs}_{\lambda 4686} = 526 \pm 27$ mÅ[2], Mathys criterion gives $\log W'''_{\rm prim} = \log W(\lambda 4388) + \log W(\lambda 4686) = 5.34 \pm 0.06$, which corresponds to a giant luminosity class for the primary. One needs $l_1 \leq 0.86$ to derive a class V. The reverse criterion may also be used: a class III for the primary implies $l_1 \geq 0.86$ or $l_2 \leq 0.14$, compatible with constraints previously deduced.

In the previous paragraph, we compared observed primary *EW*s with typical *EW*s of O9 giants and deduced that the primary was probably a giant. On the other hand, we may wonder what classification would be found if we compared the observed *EW*s with typical class V *EW*s. Indeed this would yield a larger dilution ratio for the primary and might then affect Mathys criterion. We get $l_1 = 0.80 \pm 0.06$ and therefore $\log W'''_{\rm prim} = 5.46 \pm 0.07$. The criterion gives, in this case, a main sequence class, in agreement with the hypothesis made. In consequence, Mathys criterion does not provide any further constraint as the obtained classification depends on the a priori hypothesis made to estimate the brightness ratio. Finally, we mention that the Si IV λ4089 line is much more intense in CPD – 41° 7742 primary spectrum than in typical O9 V spectra.

Typical $M_{\rm V}$ for O9 stars given by Howarth & Prinja (1989) are −5.1 and −4.2 for class III and V respectively. We adopted $M_{\rm V} = -4.54 \pm 0.26$ for CPD – 41° 7742. This results from an average of the photometry of NGC 6231 and

[2] These averaged *EW*s only take into consideration spectra that were not obtained at conjunction phases (see Sect. 5.4).

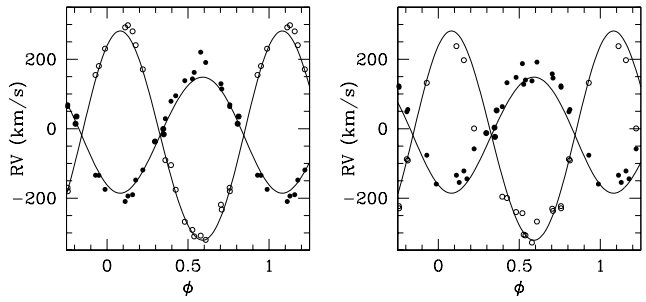

Fig. 7. Phase diagrams with C II λ4267 (left) and O II λ4367 (right) *RV* points associated to the primary (filled dots) and the secondary (open dots). The *RV* curves associated with the average He I line solution have been overplotted in both panels.

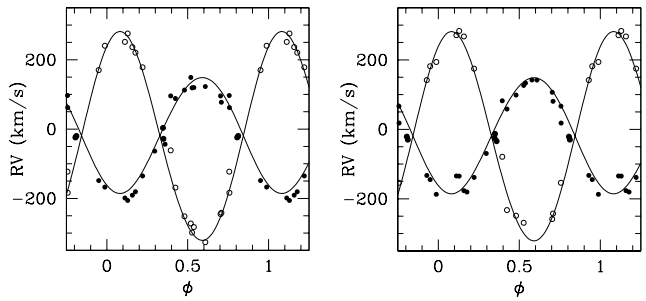

Fig. 8. Phase diagrams with Si III λ4552 (left) and Mg II λ4481 (right) *RV* points associated to the primary (filled dots) and the secondary (open dots). The *RV* curves associated with the average He I line solution have been overplotted in both panels.

of CPD – 41° 7742 published in the last ten years (Perry et al. 1991; Raboud et al. 1997; Sung et al. 1998; Baume et al. 1999). This value gives the total magnitude of the system and should therefore be considered as a lower limit for the primary component magnitude. Adopting $l_1 = 0.92 \pm 0.06$, we obtain $M_{V,1} = -4.45 \pm 0.27$. This is clearly far from a typical O9 III magnitude. If we assume that the CPD – 41° 7742 primary is indeed a main sequence star, and hence $l_1 = 0.80 \pm 0.06$, we derive $M_{V,1} = -4.30 \pm 0.27$. In this regard, the CPD – 41° 7742 primary component is thus more consistent with a main sequence classification, though all the spectral criteria indicate a giant class. At this stage it is worth to mention that the luminosity criteria based on lines that are sensitive to the surface gravity and were established for presumably single O stars may not be adapted for close binary systems.

Finally, with $V = 8.32$ and $U - B = -0.67$ (Baume et al. 1999), CPD – 41° 7742 lies at the bottom of the O9-O9.5 III clump in the colour-magnitude diagram (CMD) of NGC 6231 (see e.g. WEBDA data base: `http://obswww.unige.ch/webda/`). Its position above the main sequence is consistent with the fact that it is an SB2 binary. The previously derived combined spectral type for CPD – 41° 7742 is indeed O9 IV (Levato & Malaroda 1980). From CPD – 41° 7742's position in the CMD and from the previous discussion, we conclude that both stars belong most probably to luminosity class IV or V.

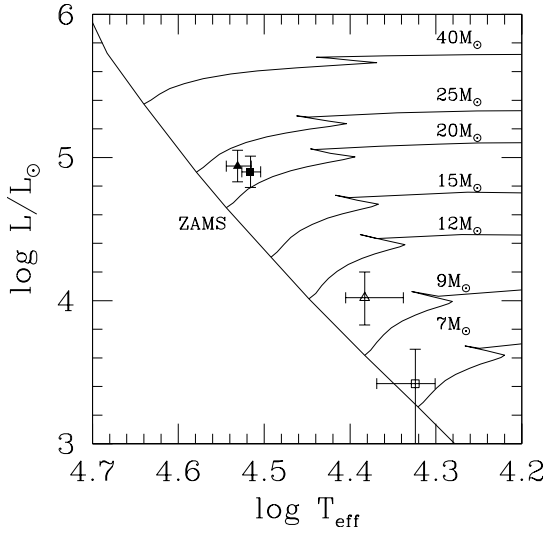

Fig. 9. Position of the primary (filled symbols) and secondary (open symbols) components of CPD – 41° 7742 in the H–R diagram. The squares (resp. triangles) refer to the positions computed by assuming giant (resp. main sequence) luminosity classes. We refer to the text for a description of the quoted error bars.

5.3. Location in the H–R diagram

Adopting the effective temperature calibration of Humphreys & McElroy (1984), the spectral types derived above (O9 III + B1 III) yield $T_{\rm eff} = 32.8\,^{33.6}_{31.9}$ kK for the primary component and $T_{\rm eff} = 21.1\,^{23.4}_{20.0}$ kK for the secondary. The quoted intervals correspond to the effective temperatures of the neighbouring subtypes. The locations of the components are plotted in the H–R diagram in Fig. 9 together with the evolutionary tracks of Schaller et al. (1992). For this purpose, we assigned $M_V = -4.54 \pm 0.26$ and we assumed that the quoted uncertainty contains both the errors on the distance modulus of the cluster and on the light variability of the system (see Sect. 5.4).

Using $l_1 = 0.92 \pm 0.06$, we finally get $\log\left(\frac{L_1^{\rm bol}}{L_\odot}\right) = 4.90\,^{5.01}_{4.79}$ and $\log\left(\frac{L_2^{\rm bol}}{L_\odot}\right) = 3.42\,^{3.66}_{2.82}$ for the bolometric luminosity of both components. The major source of uncertainty for the primary star comes from the absolute magnitude adopted. For the secondary component, it results from the uncertainty on the brightness ratio. Due to the crude method used, the above results should be taken with caution taking properly into consideration the quoted intervals especially for the secondary component. However, we can still use the information to infer constraints on the stellar radii. We obtain $R_1 = 8.7\,^{10.5}_{7.3}\,R_\odot$ and $R_2 = 3.8\,^{5.6}_{1.6}\,R_\odot$. These values are to be compared to "typical" O9–B1 giant radii of about $12-12.5\,R_\odot$. Our values are thus significantly smaller, suggesting that we are indeed dealing with luminosity class V or IV objects.

Therefore, if we assume that CPD – 41° 7742 components are indeed main sequence objects, the same reasoning with $l_1 = 0.80 \pm 0.06$ yields $\log\left(\frac{L_1^{\rm bol}}{L_\odot}\right) = 4.94\,^{5.05}_{4.83}$, $\log\left(\frac{L_2^{\rm bol}}{L_\odot}\right) = 4.02\,^{4.20}_{3.83}$ and therefore $R_1 = 8.5\,^{10.4}_{7.1}\,R_\odot$ and $R_2 = 5.8\,^{8.9}_{4.3}\,R_\odot$. Corresponding typical radii are in this case of 9.3 and 7.0 $R_\odot$ for O9 and B1 main sequence stars.

A rough interpolation of the masses from the tracks of Schaller et al. (1992) shows that the position of the giant secondary component is incompatible with the minimal mass obtained in Table 4. Adopting main sequence classifications, the relevant minimal stellar masses would yield an inclination i of about 65 to 75°.

5.4. CPD – 41° 7742, an eclipsing binary

Several authors reported a variable luminosity for the CPD – 41° 7742 system. Arentoft et al. (2001), who searched for new variable stars in NGC 6231, briefly discussed CPD – 41° 7742 and claimed to have observed incomplete eclipses but were unable to determine the times of mid-eclipses. We measured the *EW*s of two well isolated single primary lines (He II λ4686 and O III λ5592) and plotted these data versus the phase (see Fig. 10). A clear increase could be detected around $\phi \approx 0.35$, when the primary star is expected to be in front of the secondary. On the other hand, a slight dip at the other conjunction phase (i.e. around $\phi = 0.85$) may also be present while the primary is behind.

Assuming that the CPD – 41° 7742 light curve displays two eclipses as suggested above, constraints on the radii deduced in the previous section imply $i \geq 61 \pm 5°$ or $i \geq 57 \pm 5°$ according to either a giant or a main sequence class hypothesis. The quoted extreme values approximately correspond to the extreme values on the radii. $i = 61 \pm 5°$ would yield absolute masses of $24.9 \pm 3.6\,M_\odot$ and $13.8 \pm 2.0\,M_\odot$ for the primary and the secondary components respectively. The primary mass contains within its error bars typical masses of O9 III and O9 V stars as given by Howarth & Prinja (1989). We can therefore reasonably assume $i_{\rm min} \approx 60°$, in good agreement with the constraints deduced from the location of the objects in the H–R diagram.

5.5. CPD – 41° 7742, a close binary system

With a minimal orbital separation $a \sin i = (a_1 + a_2) \sin i = 22.57 \pm 0.10\,R_\odot$ and a quite high inclination as required by the presence of eclipses, CPD – 41° 7742 may be considered as a close binary system. Indeed the separation between the stellar surfaces is most probably only half of the total orbital separation. The orbital parameters given in Table 4 yield (Eggleton 1983) minimal Roche lobe (RL) radii of $R_{\rm RL} \sin i = 9.72 \pm 0.05\,R_\odot$ and $7.43 \pm 0.04\,R_\odot$ for the primary and the secondary respectively. Adopting an inclination of $i \geq 60°$ and stellar radii obtained in Sect. 5.3, we find that the filling ratio of the Roche lobes of the stars are at minimum(maximum) of about 49(72)% and 9(13)% respectively if giant classes are assumed and of 43(67)% and 31(49)% otherwise. Typical radii of giant stars of the same spectral type would require $i \leq 45°$ to avoid a Roche lobe overflow phenomenon whereas eclipses would then require $i \geq 43°$.

6. Conclusions

Using high resolution spectra, we have clearly identified the secondary orbital signature, and for the first time, we derived an accurate orbital solution for both components of CPD – 41° 7742. We showed that the orbit is slightly eccentric and obtained a period of $P = 2.44070 \pm 0.00043$ days. We further combined our data with data from the literature in order to compute a global solution for the primary. The latter turns out to be in excellent agreement with our SB2 solution. While doing this, we noticed that the data reported by García & Mermilliod (2001, GM01) were partly erroneous and should be corrected before being used. The details of this issue are explained in Sect. 4. The final set of data for the primary star covers a time range of more than 30 years. This combined analysis then suggests a period $P = 2.44062 \pm 0.00005$ days in excellent agreement with our independently derived value.

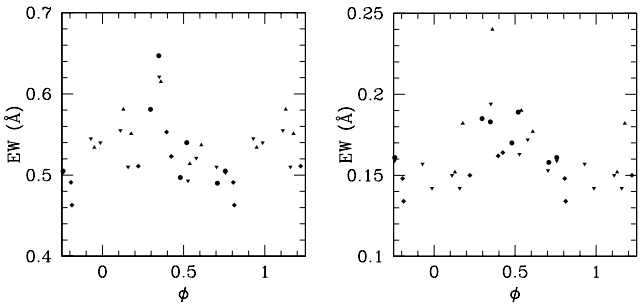

Fig. 10. He II λ4686 and O III λ5592 *EW*s plotted against the phase (as computed from the average He I line solution). Different symbols refer to different observing runs (see caption of Fig. 3).

The spectroscopic classification criteria that we applied suggest that the system is composed of a primary O9 III star and of a secondary B1 III. However, luminosity and radii obtained for the stars clearly disagree with typical values of giant stars of the same spectral types. Adopting instead a main sequence luminosity class for both objects solves much of the discrepancy. Furthermore the system is most probably too close to offer enough space for two giant stars, with typical radii, without displaying a Roche lobe overflow phenomenon.

Equivalent widths of well isolated primary lines display variations suggesting that CPD – 41° 7742 is an eclipsing binary, in agreement with incomplete observations of eclipses by Arentoft et al. (2001). Preliminary results from a photometric campaign partly dedicated to the core of NGC 6231 also confirm this idea; the results will be presented in a subsequent paper along with an X-ray lightcurve of the system. In fact, this recent discovery makes CPD – 41° 7742 an even more interesting object. Combining these new constraints with the results of the present paper will provide crucial information about the physical parameters of the system.

Finally, we emphasize that CPD – 41° 7742 is the second known SB2 eclipsing early-type binary system of the NGC 6231 cluster (the first being HD 152248, Sana et al. 2001). The results of these papers together with other papers in preparation on the early-type objects of NGC 6231 will help to constrain both early-type evolutionary models as well as binary formation theories of these objects.

Acknowledgements. We are grateful to the referee, Dr. J. C. Mermilliod, for his helpful comments and suggestions. We thank Jean Manfroid and Pierre Royer for communicating preliminary results of

their photometric campaign. We also acknowledge support from the PRODEX XMM-OM and Integral Projects, contracts P4/05 and P5/36 “Pôle d’Attraction Interuniversitaire” (Belgium).

References

Arentoft, T., Sterken, C., Knudsen, M. R., et al. 2001, A&A, 380, 599
Baume, G., Vázquez, R. A., & Feinstein, A. 1999, A&AS, 137, 233
Braes, L. L. E. 1967, Bulletin of the Astronomical Institute of the Netherlands, Supp. Ser., 2, 1
Conti, P. S. 1973, ApJ, 179, 181
Conti, P. S., & Alschuler, W. R. 1971, ApJ, 170, 325
Conti, P. S., Leep, E. M., & Lorre, J. J. 1977, ApJ, 214, 759
Deharveng, L., Zavagno, A., Salas, L., et al. 2003, A&A, 399, 1135
Didelon, P. 1982, A&AS, 50, 199
Eggleton, P. P. 1983, ApJ, 268, 368
García, B., & Mermilliod, J. C. 2001, A&A, 368, 122 (GM01)
Gimenez, A. 1996, in The origins, evolution, and destinies of binary stars in clusters, ed. E. F. Milone, & J. C. Mermilliod, ASP Conf. Ser., 90, 109
Gosset, E., Royer, P., Rauw, G., Manfroid, J., & Vreux, J.-M. 2001, MNRAS, 327, 435
Heck, A., Manfroid, J., & Mersch, G. 1985, A&AS, 59, 63 (HMM)
Hensberge, H. 2002, Evaluation of FEROS Pipeline, http://www.ls.eso.org/lasilla/Telescopes/2p2T/E1p5M/FEROS/Reports/index.html
Hill, G., Crawford, D. L., & Barnes, J. V. 1974, AJ, 79, 1271 (HCB74)
Howarth, I. D., & Prinja, R. K. 1989, ApJS, 69, 527
Humphreys, R. M., & McElroy, D. B. 1984, ApJ, 284, 565
Kukarkin, B. V., Kholopov, P. N., Pskovsky, Y. P., et al. 1971, General Catalogue of Variable Stars, 3rd ed.
Lafler, J., & Kinman, T. D. 1965, ApJS, 11, 216 (L&K)
Levato, H., & Malaroda, S. 1980, PASP, 92, 323
Levato, H., & Morrell, N. 1983, ApL, 23, 183 (LM83)
Mathys, G. 1988, A&AS, 76, 427
Maeder, A., & Meynet, G. 1995, Msngr, 80, 19
Maeder, A., & Meynet, G. 2000, A&A, 361, 159
Mermilliod, J. C. 2003, private communication
Moore, C. E. 1959, in A Multiplet Table of Astrophysical Interest, Technical Note 36, National Bureau of Standards (Washington: U. S. Department of Commerce)
Perry, C. L., Hill, G., Younger, P. F., & Barnes, J. V. 1990, A&AS, 86, 415 (PHYB90)
Perry, C. L., Hill, G., & Christodoulou, D. M. 1991, A&AS, 90, 195
Raboud, D., Cramer, N., & Bernasconi, P. A. 1997, A&A, 325, 167
Rauw, G., Sana, H., Gosset, E., et al. 2000, A&A, 360, 1003
Sana, H., Rauw, G., & Gosset, E. 2001, A&A, 370, 121
Schaller, G., Schaerer, D., Meynet, G., & Maeder, A. 1992, A&AS, 96, 269
Seggewiss, W. 1968, Veroeff. Astron. Inst. Bonn, 79, 1
Struve, O. 1944, ApJ, 100, 189
Sung, H., Bessell, M. S., & Lee, S.-W. 1998, AJ, 115, 734
Underhill, A. B. 1994, ApJ, 420, 869
Walborn, N. R., & Fitzpatrick, E. L. 1990, PASP, 102, 379 (WF90)
Wolfe, R. H. Jr., Horak, H. G., & Storer, N. W. 1967, in Modern Astrophysics, ed. M. Hack, Gordon, & Breach (New York), 251